online data

Crystal structure of human phosphoribosylpyrophosphate synthetase 1 reveals a novel allosteric site

Sheng LI*†, Yongcheng LU*†, Baozhen PENG* and Jianping DING*[1]

*State Key Laboratory of Molecular Biology, Institute of Biochemistry and Cell Biology, Shanghai Institutes for Biological Sciences, Chinese Academy of Sciences, 320 Yue-Yang Road, Shanghai 200031, China, and †Graduate School of Chinese Academy of Sciences, 320 Yue-Yang Road, Shanghai 200031, China

PRPP (phosphoribosylpyrophosphate) is an important metabolite essential for nucleotide synthesis and PRS (PRPP synthetase) catalyses synthesis of PRPP from R5P (ribose 5-phosphate) and ATP. The enzymatic activity of PRS is regulated by phosphate ions, divalent metal cations and ADP. In the present study we report the crystal structures of recombinant human PRS1 in complexes with SO_4^{2-} ions alone and with ATP, Cd^{2+} and SO_4^{2-} ions respectively. The AMP moiety of ATP binds at the ATP-binding site, and a Cd^{2+} ion binds at the active site and in a position to interact with the β- and γ-phosphates of ATP. A SO_4^{2-} ion, an analogue of the activator phosphate, was found to bind at both the R5P-binding site and the allosteric site defined previously. In addition, an extra SO_4^{2-} binds at a site at the dimer interface between the ATP-binding site and the allosteric site. Binding of this SO_4^{2-} stabilizes the conformation of the flexible loop at the active site, leading to the formation of the active, open conformation which is essential for binding of ATP and initiation of the catalytic reaction. This is the first time that structural stabilization at the active site caused by binding of an activator has been observed. Structural and biochemical data show that mutations of some residues at this site influence the binding of SO_4^{2-} and affect the enzymatic activity. The results in the present paper suggest that this new SO_4^{2-}-binding site is a second allosteric site to regulate the enzymatic activity which might also exist in other eukaryotic PRSs (except plant PRSs of class II), but not in bacterial PRSs.

Key words: allosteric site, nucleotide synthesis, oligomerization, PRPP synthetase, regulation mechanism.

INTRODUCTION

PRPP (phosphoribosylpyrophosphate) synthetases (ATP: D-ribose-5-phosphate pyrophosphotransferase; EC 2.7.6.1) are a family of enzymes that catalyse the synthesis of PRPP from ATP and R5P (ribose 5-phosphate) by transferring the β,γ-diphosphoryl moiety of ATP to the C1-hydroxy group of R5P [1–3]. PRPP is a key intermediate of metabolism that is required for synthesis of the purine and pyrimidine nucleotides, the pyridine nucleotide cofactors NAD and NADP, and the amino acids histidine and tryptophan [4,5]. Superactivity of PRS (PRPP synthetase) is an inherited X-chromosome-linked disorder [6] and the excessive enzymatic activity is associated with uric acid overproduction, gout and neurodevelopmental abnormalities [7–10]. Three classes of PRSs have been reported which are divided based on their dependence on phosphate ions for activity, their allosteric regulation mechanism and their diphosphoryl donor specificity [11–15]. Most PRSs belong to class I, which require Mg^{2+} and phosphate for enzymatic activity, but can be inhibited allosterically by ADP and possibly other nucleotides [16–24]. Class II PRSs are found specifically in plants which are not dependent on phosphate for activity and lack an allosteric site for ADP [11,12]. While class I PRSs transfer the diphosphoryl group only from ATP or dATP to R5P [17,19], class II PRSs have a much broader specificity for a diphosphoryl donor, including ATP, dATP, UTP, CTP and GTP [12,13]. Recently, a novel class III PRS has been identified from *Methanocaldococcus jannaschii* which is activated by phosphate and uses ATP and dATP as a diphosphoryl donor, but also lacks an allosteric site for ADP [15].

Mg^{2+} forms a complex with ATP (Mg–ATP) to act as the actual substrate of the enzyme although other divalent cations, such as Mn^{2+}, Ni^{2+}, Co^{2+} or Cd^{2+} can serve as substitutes for Mg^{2+} with relatively lower activity [16,17,19,22,24–26]. Phosphate has multiple effects on the activity and structure of the enzyme. It usually acts as an activator for the activity of bacterial and mammalian PRSs although SO_4^{2-} can mimic the effect of phosphate at approx. 10-fold higher concentrations [14,16,19,22,24,27]. However, phosphate or SO_4^{2-} has to compete with the inhibitor ADP at the same allosteric site for their function. On the other hand, at high concentrations both phosphate and SO_4^{2-} can exhibit an inhibitory effect because of their competitive binding at the R5P binding site [14]. ADP functions as the most potent inhibitor in either a competitive or allosteric manner depending on the presence and concentration of substrates [18,21,22,24,28]. The competitive inhibition by ADP is owing to its competitive binding against ATP at the ATP binding site and the allosteric inhibition acts through its competitive binding with phosphate at the allosteric site [26,29].

Structural studies of PRSs from *Bacillus subtilis* [14,30] and *M. jannaschii* [15] have been performed to characterize the binding sites for substrates, activator and inhibitor. Both PRSs consist of two domains related by a pseudo 2-fold symmetry, and each domain assumes the type I phosphoribosyltransferase fold. bsPRS (*B. subtilis* PRS) forms a hexamer in the crystal structure and is organized as a propeller with the N-terminal domains at the centre and the C-terminal domains at the outside. The catalytic active site, consisting of the ATP binding site and the R5P binding site, is located at the interface of two domains of one subunit, and

Abbreviations used: PRPP, phosphoribosylpyrophosphate; PRS, PRPP synthetase; bsPRS, *Bacillus subtilis* PRPP synthetase; hPRS, human PRPP synthetase; mjPRS, *Methanocaldococcus jannaschii* PRPP synthetase; PPi, pyrophosphate; R5P, ribose 5-phosphate; rmsd, root mean square deviation; mATP, α,β-methylene ATP; mADP, α,β-methylene ADP.

[1] To whom correspondence should be addressed (email jpding@sibs.ac.cn).

The structures of the wild-type, S132A and Y146M mutant hPRS1 · SO_4^{2-} complexes and the wild-type hPRS1 · ATP · SO_4^{2-} · Cd^{2+} complex have been deposited with the RCSB Protein Data Bank under accession codes 2H06, 2H07, 2H08 and 2HCR respectively.

the allosteric site for phosphate and ADP is located at the interface between three subunits of the hexamer [14,30]. mjPRS (*M. jannaschii* PRS) has a tetrameric quaternary structure with two homodimers stacking onto each other, and the active site is located at the domain interface of the subunit, but no allosteric site is found [15].

hPRSs (human PRPP synthetases) have three isoforms that share very high sequence identity (95.0 % between hPRS1 and hPRS2; 94.3 % between hPRS1 and hPRS3; and 91.2 % between hPRS2 and hPRS3 respectively) [31–34]. *hPRS1* and *hPRS2* genes are located on the X chromosome and are expressed in a wide range of tissues, but *hPRS3* is an autosomal gene expressed specifically in testis. hPRS1 contains 318 amino acids and shares a moderate sequence identity with bsPRS (47 % identity and 67 % similarity respectively). It requires phosphate for activation and uses Mg^{2+} for activity [17,25,35]. The crystallization of hPRS1 has recently been reported [36]. In the present paper we describe the crystal structures of hPRS1 in complexes with SO_4^{2-} ions and with ATP, Cd^{2+} and SO_4^{2-} ions respectively. hPRS1 has an overall structure similar to that of bsPRS. Interestingly, in addition to binding at the R5P binding site and the allosteric site defined previously in bsPRS, an extra SO_4^{2-} ion is found to bind at a new allosteric site at the dimer interface. Structural and biochemical data together reveal new insights into the allosteric regulatory mechanism of hPRS1 and possibly other eukaryotic PRSs (except for class II plant PRSs).

MATERIALS AND METHODS

Cloning, expression and purification of hPRS1

The *hPRS1* gene encoding the full-length hPRS1 protein (318 amino acids) was obtained from the cDNA library of human CD34+ haematopoietic stem/progenitor cells [37]. The gene was cloned into the NdeI and XhoI restriction sites of the pET-22b(+) expression plasmid (Novagen) which inserts a His tag (LEHHHHHH) at the C-terminus. The plasmid was transformed into and expressed in *Escherichia coli* BL21(DE3) strain (Novagen). The bacterial cells were grown in Luria–Bertani medium supplemented with ampicillin (50 μg/ml) at 37 °C until D_{600} reached 0.8. After 8 h of expression induced with 0.5 mM IPTG (isopropyl-β-D-thiogalactopyranoside) at 20 °C, the cells were collected by centrifugation at 4000 ***g*** for 10 min and suspended in lysis buffer [50 mM NaH_2PO_4 (pH 8.0), 1 M NaCl, 15 % (w/v) glycerol, 5 mM 2-mercaptoethanol and 1 mM PMSF]. The cells were further lysed on ice by sonication and the cell debris was precipitated by centrifugation at 13 000 ***g*** for 40 min.

Protein purification was carried out by affinity chromatography using a 5 ml Ni–agarose column (Amersham Pharmacia) and an ion-exchange method using a 1 ml ANX weak ion-exchange column (Amersham Pharmacia). The lysis supernatant was loaded onto the Ni–agarose column equilibrated with the lysis buffer which was then washed with a washing buffer (lysis buffer supplemented with 75 mM imidazole) to remove non-specific binding proteins. The target protein was eluted with an elution buffer [50 mM NaH_2PO_4 (pH 8.0), 1 M NaCl, 15 % (w/v) glycerol and 75 mM EDTA]. This protein sample was dialysed against buffer A [20 mM NaH_2PO_4 (pH 8.0)] at 20 °C for 3 h and then loaded onto the ANX column. The column was washed with buffer A containing gradually increased concentrations of 1 M NaCl up to 50 % (v/v) in 20 min and the target protein was washed down at 20–35 % concentration of 1 M NaCl. The peak fractions were collected, concentrated and then stored at −70 °C in buffer B (buffer A supplemented with 400 mM NaCl) for biochemical and structural studies. All purification steps were carried out at 4 °C unless otherwise stated to minimize potential proteolysis of the protein. Reducing SDS/PAGE analyses of the protein sample showed a single band at approx. 35 kDa. DLS (dynamic light scattering) analysis was performed to characterize the aggregation state of the protein in solution (at a protein concentration of approx. 2 mg/ml). Expression plasmids of mutant hPRS1 were generated from the vector containing the wild-type enzyme using the QuikChange Site-Directed Mutagenesis Kit (Stratagene) and the sequences of these genes were confirmed by DNA sequencing. The mutant enzymes were expressed and purified following the same procedures as for the wild-type enzyme.

Crystallization and diffraction data collection

Crystallization was performed at 20 °C using the hanging-drop vapour diffusion method. Initial crystallization trials were performed using screening kits from Hampton Research. Protein solution (2 μl) was mixed with 2 μl of the reservoir solution. After several rounds of optimization, cluster-shaped crystals were obtained at the reservoir solution containing 100 mM citric acid (pH 4.15) and 1.3 M $(NH_4)_2SO_4$. The hPRS1 mutants were crystallized in similar conditions following the same procedure, except that the pH was varied. Crystals of the hPRS1 · ATP · SO_4^{2-} · Cd^{2+} (quaternary complex) were obtained by adding a solution containing ATP and $CdCl_2$ to a crystallization drop containing pre-grown crystals of the hPRS1 · SO_4^{2-} complex with the final concentration of about 10 mM for both ATP and $CdCl_2$. This soaking process was allowed to equilibrate for more than 48 h before data collection. All of these crystals belong to space group *R*3. The diffraction data of wild-type and Y146M hPRS1 were collected from flash-cooled crystals at −176 °C using synchrotron radiation at beamline BL-6A at the Photon Factory, Japan. The diffraction data of S132A hPRS1 and the quaternary complex of hPRS1 were collected from flash-cooled crystals at −170 °C using an in-house Rigaku R-AXIS IV++. The statistics of diffraction data are summarized in Table 1.

Structure determination and refinement

The structure of wild-type hPRS1 was solved with the MR (molecular replacement) method as implemented in the program CNS [38] using the dimeric bsPRS structure as the search model [14]. The structures of the two mutants and the quaternary complex were determined with MR using the wild-type hPRS1 structure as the search model. Structure refinement was carried out using CNS and REFMAC5 [39] and model building was facilitated using the program O [40]. There are two monomers in the asymmetric unit; therefore strict 2-fold NCS (non-crystallographic symmetry) constraints were applied in the early stage of refinement, but released in the later stage of refinement. In the initial difference Fourier maps there was strong electron density at both the R5P binding site and the allosteric site defined in the structure of the bsPRS · SO_4^{2-} complex [14]. The position and shape of the electron density match the SO_4^{2-} ion very well and therefore they were modelled as SO_4^{2-} ions. In addition, one extra SO_4^{2-} ion was found to bind at the homodimer interface in each subunit with well-defined electron density and co-ordination geometry which appeared to be a second allosteric site (see Results and discussion section). In the quaternary complex, there was well-defined electron density for the AMP moiety of an ATP molecule at the ATP binding site of each subunit, but very poor density for the β- and γ-phosphate moieties of ATP and therefore we modelled only the AMP moiety of ATP in the final model. In addition, there was electron density for a metal ion at the ATP binding site which occupies a similar position to that in the bsPRS structure [30].

Table 1 Statistics of diffraction data and structure refinement

	Wild-type	S132A	Y146M	ATP · SO_4^{2-} · Cd^{2+}
Diffraction data statistics				
Resolution (Å)	50.00–2.20 (2.28–2.20)*	25.00–2.20 (2.28–2.20)	50.00–2.50 (2.59–2.50)	25.00–2.20 (2.28–2.20)
Space group	*R*3	*R*3	*R*3	*R3*
Unit cell parameters (Å)				
a=*b*	169.68	170.34	169.91	170.24
c	61.59	61.72	61.71	61.82
Mosaicity	0.54	0.77	0.52	0.75
Observed reflections	108475	139709	103854	193805
Unique reflections [$I/\sigma(I)>0$]	33517	33483	22978	32945
Average redundancy	3.2 (3.1)	4.2 (4.1)	4.5 (4.5)	5.9 (5.7)
Completeness (%)	99.9 (99.9)	98.8 (97.7)	100.0 (100.0)	97.1 (96.8)
Average $\langle I/\sigma(I)\rangle$	16.8 (2.4)	8.6 (2.3)	16.6 (3.3)	7.9 (2.1)
R_{rmerge} (%)†	7.4 (55.2)	6.7 (32.5)	9.2 (47.5)	7.4 (35.9)
Refinement statistics				
Number of reflections [$F_o \geqslant 0\sigma(F_o)$]				
Working set	31841	31803	21823	31269
Free R set	1676	1680	1155	1672
R factor‡	0.212	0.218	0.207	0.205
Free R factor	0.245	0.254	0.257	0.254
Subunits/asymmetric unit	2	2	2	2
Total protein atoms	4691	4689	4683	4691
Total ligand atoms	30	30	30	78
Total solvent atoms	183	132	164	144
Average B factor of all atoms (Å^2)	43.8	39.6	41.0	36.4
Protein main chain	42.3	38.2	40.0	35.4
Protein side chain	45.3	41.1	41.9	37.0
Ligands	52.8	47.9	54.3	51.6
Waters	45.0	37.5	40.3	33.9
rmsd				
Bond lengths (Å)	0.007	0.006	0.010	0.008
Bond angles (°)	1.2	1.2	1.4	1.2
Dihedral angles (°)	23.6	23.6	26.5	25.5
Improper angles (°)	0.78	0.76	1.51	1.50
Ramachandran plot (%)				
Most favoured regions	89.4	89.4	88.3	89.7
Additional allowed regions	10.3	10.5	11.2	9.5
Generously allowed regions	0.4	0.2	0.5	0.7
Luzzati atomic positional error (Å)	0.27	0.27	0.28	0.27

* The numbers in parentheses refer to the highest resolution shell.

† $Rmerge = \Sigma_{hkl}\Sigma_i|I_i(hkl)_I - \langle I(hkl)\rangle|/\ \Sigma_{hkl}\Sigma_i I_i(hkl)$.

‡ R factor $= ||F_o| - |F_c||/|F_o|$.

Since only the Cd^{2+} ion existed in the crystallization solution, we modelled the metal ion as a Cd^{2+} ion with its occupancy being adjusted to 0.6 according to the difference density. The statistics of structure refinement are summarized in Table 1.

Enzymatic activity assay

The enzymatic activity of wild-type and mutant hPRS1 was determined by the ^{32}P transfer assay performed at 37 °C in 50 mM triethanolamine (pH 8.0) using a modified method based on that described previously [41]. First the protein was dialysed against a dialysis buffer [50 mM triethanolamine (pH 8.0) and 1 mM ATP] at 20 °C for 2 h, and then diluted to 0.1 mg/ml with the same buffer. The reaction solution containing 2 μl of the enzyme and 18 μl of the reaction buffer [50 mM triethanolamine, 2 mM ATP, 5 mM R5P, 5 mM $MgSO_4$, 0 or 100 μM ADP and phosphate of varying concentrations (0, 5 and 50 mM)] was incubated at 37 °C and then 10 μl aliquots of the reaction solution were withdrawn after 5 min and mixed with 5 μl of 0.33 M formic acid. The mixture (1.5 μl) was applied to poly(ethyleneimine) sheets which were developed in 0.85 M KH_2PO_4 (pH 3.4) at 4 °C and then dried and exposed using a PhosphorImager (Molecular Dynamics). In the control experiments, phosphate was omitted from the reaction solution. All experiments were repeated at least three times under the same conditions.

RESULTS AND DISCUSSION

Overall structure of hPRS1

The crystal structure of wild-type hPRS1 was determined using the MR method. The final structure model contains two hPRS1 subunits forming a homodimer, six SO_4^{2-} ions and 183 water molecules in the asymmetric unit (Figure 1). Subunit A contains 305 amino acid residues from Asn^3 to Phe^{313} except for Lys^{197}–Val^{202}, and subunit B contains 308 amino acid residues from Asn^3 to Pro^{317} except for Arg^{196}–Val^{202}. The two NCS-related subunits in the asymmetric unit are essentially identical as revealed by superposition of all corresponding Cα atoms in each subunit [an rmsd (root mean square deviation) of 0.54 Å (1 Å = 0.1 nm)]. The statistics of structure refinement and the protein model are summarized in Table 1.

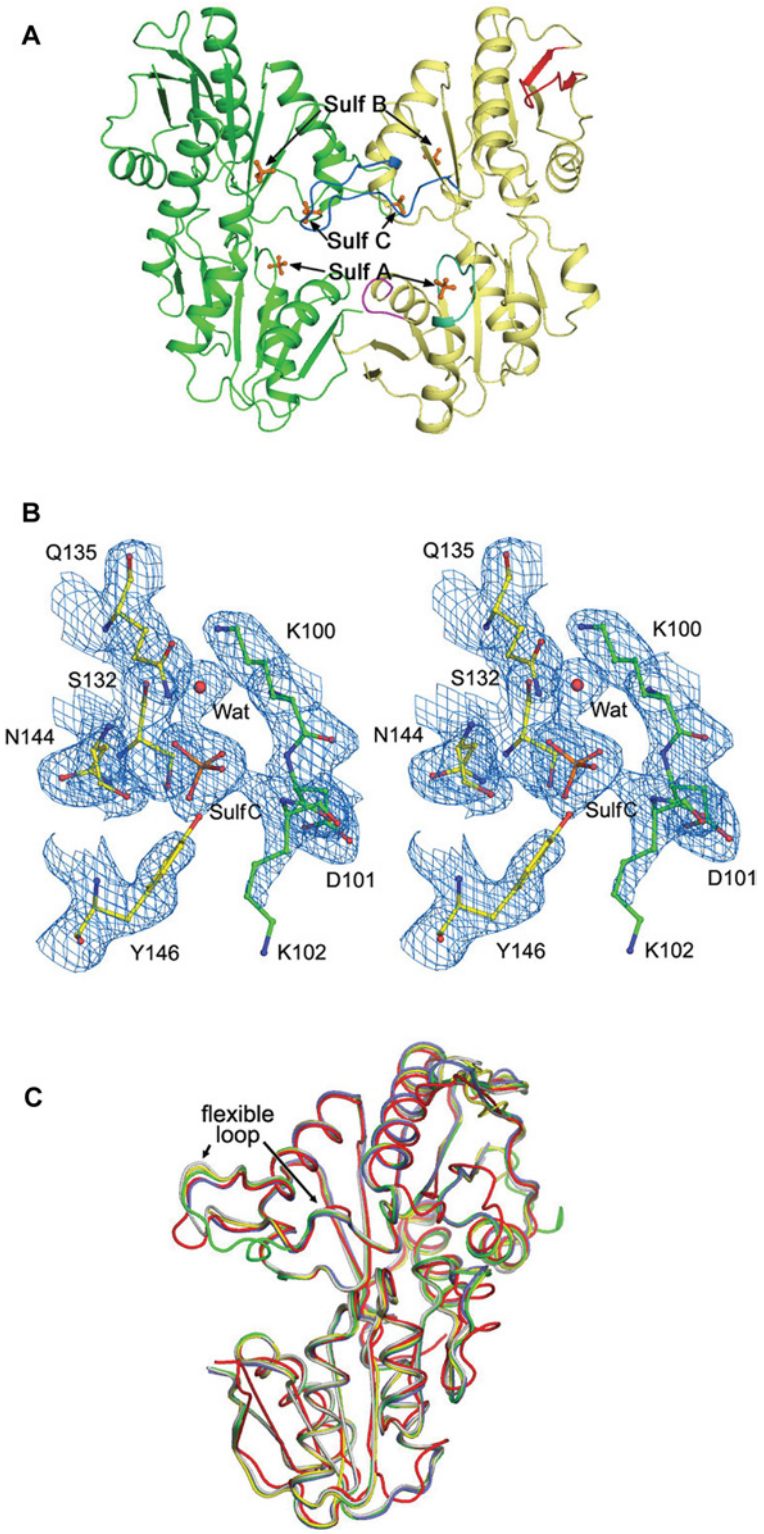

Figure 1 Structure of human PRS1

(**A**) Overall structure of hPRS1. There are two hPRS1 subunits (coloured in green and yellow respectively) in an asymmetric unit forming a homodimer. Each subunit is composed of two domains related by a pseudo two-fold symmetry and each domain assumes the type I phosphoribosyltransferase fold. The flexible loop involved in ATP binding is shown in blue, the PPi binding loop in magenta, the R5P binding loop in cyan and the flag region in red (for clarity, only one subunit is colour-coded). The bound SO_4^{2-} ions are shown with ball-and-stick models: Sulf A, the SO_4^{2-} ions in the R5P binding sites; Sulf B, the SO_4^{2-} ions in the previously defined allosteric sites; Sulf C, the SO_4^{2-} ions in the new allosteric sites. For all detailed panels in Figures 2 and 3, the viewpoints are roughly perpendicular to the paper plane of this overview. (**B**) Representative SIGMMA-weighted $2F_0 - F_c$ map (1σ contour level) in the new allosteric site. The SO_4^{2-} ion and surrounding residues are shown with ball-and-stick models. (**C**) Superposition of hPRS1 with bsPRS. The hPRS1 · SO_4^{2-} structure is shown in red, the bsPRS · SO_4^{2-} structure (PDB code 1DKR) with the closed conformation in green and the open conformation in blue, the bsPRS · mATP · SO_4^{2-} · Cd^{2+} structure (PDB code 1IBS) in yellow, and the bsPRS · mADP structure PDB code 1DKU) in white.

Structural comparison indicates that the overall structure of hPRS1 is very similar to that of bsPRS [14,30] [an rmsd of 1.02 Å compared with the bsPRS · SO_4^{2-} complex, 1.18 Å compared with the bsPRS · mADP (α, β-methylene ADP) complex and 1.06 Å compared with the bsPRS · mATP · SO_4^{2-} · Cd^{2+} (mATP, α,β-methylene ATP) complex respectively] (Figure 1C and Supplementary Figure S1 at http://www.BiochemJ.org/bj/401/bj4010039add.htm). Like bsPRS, hPRS1 consists of two domains with a similar sandwich-like α/β structure (Figure 1A). At the N-terminal domain, the central five-stranded parallel β-sheet is surrounded by four α-helices and one 3_{10}-helix; at the C-terminal domain, it is flanked by two α-helices on one side and three α-helices on the other. Both domains also contain a short anti-parallel β-sheet that protrudes from the central core. The strong conservation of the overall structure of two different PRSs with a moderate sequence homology underscores the functional importance of the enzymes in the metabolism. Despite the overall structural similarity, there are a few notable conformational differences between the two PRSs (Figure 1C). Region Gln^{278}–His^{283} in hPRS1 forms an α-helix (α8), whereas the equivalent region (Leu^{280}–Lys^{285}) in bsPRS adopts a loop conformation. The region Ser^{160}–Asn^{164} in hPRS1 forms a short 3_{10}-helix (η2), whereas the corresponding region in bsPRS forms an extended loop. In addition, conformational differences are observed in several loops, including Ser^{10}–Asp^{14}, Ser^{58}–Gly^{61} and Tyr^{97}–Thr^{113} (the flexible loop).

Quaternary structure of hPRS1

PRSs normally form oligomers in solution and aggregation appears to be necessary for the enzymatic activity [17,19,42]. In the bsPRS structures, the enzyme forms a hexamer and both the catalytic active site and the allosteric regulatory site are formed by conserved residues from more than one subunit, leading to the suggestion that the hexamer is the physiological functional unit for PRSs [14,30]. The quaternary structure of hPRS1 is also similar to that of bsPRS: three homodimers form a hexamer in a propeller shape with a 32 point group symmetry, the N-terminal domains form the inner circle close to the 3-fold axis and the C-terminal domains form the blades towards the outside, further supporting the notion that the hexameric form of the enzyme is the minimal physiological functional unit (see Supplementary Figure S2 at http://www.BiochemJ.org/bj/401/bj4010039add.htm). This arrangement, however, is different from that of mjPRS which forms a tetramer with two homodimers stacking onto each other [15]. There are two types of inter-subunit interface in the hexamer: the interface between the two subunits of the homodimer in the asymmetric unit (designated as the dimer interface) and the interface between the two subunits of the neighbouring homodimers near the 3-fold axis (designated as the trimer interface). Contacts between adjacent subunits are very tight, burying 3878 $Å^2$ or 27.7 % of the accessible surface area of each subunit (among them the dimer interface buries 1570 $Å^2$ or 11.2 % and the trimer interface buries 1845 $Å^2$ or 13.2 % respectively). Both dimer and trimer interfaces involve extensive hydrophobic and hydrophilic interactions between highly conserved residues. Genetic and biochemical studies have shown that hPRS superactivity can be caused by a number of mutations in hPRS1 resulting in alteration of the allosteric regulatory mechanisms of activation by phosphate and inhibition by ADP [9,10]. Structural analysis of hPRS1 indicates that the majority of those mutations (including N114S, D183H, A190V and H193Q) are located at the dimer interface and their changes would probably affect the formation of the homodimer and thus the allosteric regulatory site and the enzymatic activity.

The active site

The active site of PRS comprises the binding sites for ATP and R5P. Like bsPRS, the ATP binding site of hPRS1 is located at the interface of two domains of one subunit and is composed of conserved residues of primarily three structural elements, namely the flexible loop (residues Phe^{92}–Ser^{108}, corresponding to residues Tyr^{97}–Thr^{113} of bsPRS), the PPi (pyrophosphate) binding loop (residues Asp^{171}–Gly^{174}, corresponding to residues Asp^{174}–Gly^{177} of bsPRS), and the flag region (residues Val^{30}–Ile^{44} of an adjacent subunit, corresponding to residues Cys^{35}–Ile^{49} of bsPRS) (Figure 2A). In the hPRS1 · ATP · SO_4^{2-} · Cd^{2+} complex structure, only the AMP moiety of ATP and a Cd^{2+} ion were found to bind at the ATP binding site while the PPi moiety of ATP was disordered, which is similar to the bsPRS · mATP · SO_4^{2-} · Cd^{2+} complex [30]. The bound AMP has interactions with residues Arg^{96}, Gln^{97}, Asp^{101} and His^{130} of one subunit and Phe^{35}, Asn^{37} and Glu^{39} of the other subunit, which are highly conserved in all PRSs (Figure 2B). The adenine N1 atom of AMP forms a hydrogen bond with the side chain of Arg^{96} and the N6 atom forms two hydrogen bonds with the side chains of Asn^{37} and Glu^{39} respectively. The ribose 2′- and 3′-hydroxy groups of AMP form two hydrogen bonds with the side chains of Gln^{97} and Asp^{101} respectively. The α-phosphate group of AMP has hydrogen-bonding interactions with the side chains of Lys^{99} and His^{130}. In addition, the side chains of Lys^{99} and Lys^{176} are in positions to interact with the β- and γ-phosphates of ATP. In the bsPRS structure, Arg^{104} (equivalent to Lys^{99} of hPRS1) appears to have a similar function; however, Ser^{179} (equivalent to Lys^{176} of hPRS1) has a much shorter side chain and may have no interaction with the PPi group of ATP. Biochemical data have shown that Lys^{197} and Arg^{199} of the flexible catalytic loop in bsPRS play important roles in stabilization of the transition state and their mutations can drastically reduce the V_{max} of the enzyme [43]. In the hPRS1 structures, the majority of the flexible catalytic loop remains disordered and the resolved parts adopt a conformation similar to that observed in the bsPRS · mATP · SO_4^{2-} · Cd^{2+} complex [30]. The side chain of Arg^{196} (corresponding to Arg^{199} of bsPRS) is pointed towards the bound ATP and the distance between the guanidinium group of Arg^{196} and the α-phosphate of ATP is about 7.4 Å. Therefore it is very probable that the side chain of Arg^{196} is involved in the interaction with the PPi and stabilization of the transition state. Though the side chain of Lys^{194} (corresponding to Lys^{197} of bsPRS) is pointed away from the substrate, it is possible that a conformational change of the flexible catalytic loop as observed in the bsPRS structure may take place, so it could also be involved in the stabilization of the transition state of the substrate.

Biochemical data show that a Mg^{2+} ion can steadily bind to both β- and γ-phosphates of ATP, forming an Mg–ATP complex to act as the actual substrate of the enzyme [16,19,25,44]. In the hPRS1 · ATP · SO_4^{2-} · Cd^{2+} complex structure, the bound Cd^{2+} ion has four ligands from the bidentate carboxylates of both Asp^{171} and Asp^{220} (equivalent to Asp^{174} and Asp^{223} of bsPRS respectively), and is in a position to interact with the β- and γ-phosphates of ATP, but is about 5 Å away from the α-phosphate (Figure 2B). It is possible that this Cd^{2+} ion might mimic the Mg^{2+} ion in the Mg–ATP complex in the catalysis. In the bsPRS · mATP · SO_4^{2-} · Cd^{2+} complex structure, a second Cd^{2+} ion binds near His^{135} (corresponding to His^{130} of hPRS1) which is suggested to be the binding site of a free cation in the catalytic reaction [30]. However, no Cd^{2+} ion was found to bind at the equivalent site in the hPRS1 complex.

The flexible loop of bsPRS exhibits the largest conformational change in different structures: it is partially disordered when either a SO_4^{2-} ion is bound at the allosteric site and/or mATP is bound

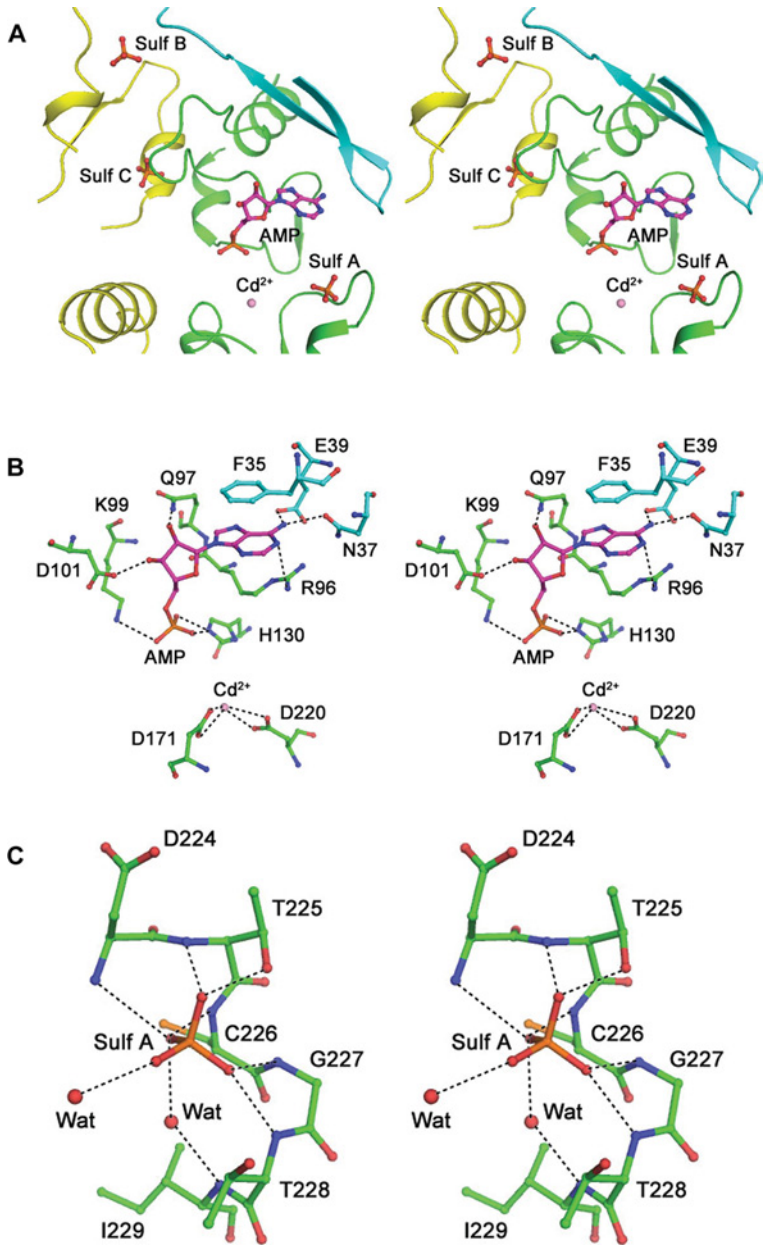

Figure 2 Structure of the catalytic active site in the hPRS1 · ATP · SO_4^{2-} · Cd^{2+} complex

(**A**) Ribbon diagram showing the relative locations of the ATP binding site, the R5P binding site (Sulf A), the previously defined allosteric site (Sulf B), and the new allosteric site (Sulf C). The AMP moiety of the bound ATP at the ATP binding site is shown with a ball-and-stick model, and the three SO_4^{2-} ions are shown in gold. The bound Cd^{2+} ion is shown with a purple sphere. Structural elements of the three subunits forming the catalytic active site are shown in yellow, green and cyan respectively. (**B**) Interactions of the AMP moiety of ATP with the surrounding residues at the ATP binding site. The hydrogen-bonding interactions are indicated with thin dashed lines. (**C**) Interactions of the SO_4^{2-} ion (Sulf A) with the surrounding residues at the R5P binding site.

at the active site, but is entirely ordered when only mADP is bound at the allosteric site [14]. However, in the structures of the hPRS1 complexes in the absence and presence of ATP, the flexible loop assumes a well-defined, open conformation similar to that observed in the bsPRS · mATP · SO_4^{2-} · Cd^{2+} structure (Figure 1C). This conformational difference appears to be correlated with the binding of the SO_4^{2-} ion at the novel allosteric site and plays an important role in the regulation of the enzymatic activity (see discussion later).

The R5P binding site of bsPRS was identified to be localized in the region of Asp^{223}–Thr^{231} of the C-terminal domain of each subunit based on structural similarity with type I phosphoribosyltransferases [45,46]. Similarly, the R5P binding loop of hPRS1 can be defined as residues Asp^{220}–Thr^{228}. In the structures of both hPRS1 · SO_4^{2-} and hPRS1 · ATP · SO_4^{2-} · Cd^{2+} complexes, a SO_4^{2-} ion is bound at the R5P binding site and occupies the position of the 5′-phosphate of R5P, similar to that in the bsPRS · SO_4^{2-} complex [14]. The SO_4^{2-} ion has direct hydrogen-bonding interactions with the main chain amides of the strictly conserved residues Asp^{224}, Thr^{225}, Cys^{226}, Gly^{227} and Thr^{228}, and the side chains of Thr^{225} and Thr^{228}, as well as two water molecules (Figure 2C).

Compared with the hPRS1 · SO_4^{2-} structure, the binding of ATP induces movement of the tip of the flag region about 2–3 Å closer

to the ATP binding site to interact with the adenine moiety of ATP. In addition, the side chain of Gln^{97} of the flexible loop rotates about 180° to form a hydrogen bond with the ribose 2′-hydroxy group of ATP. It is also noteworthy that the side chain of the strictly conserved Arg^{96} of the flexible loop at the ATP binding site has two different conformations in the two subunits of the hPRS · SO_4^{2-} complex: one assumes a conformation pointing towards the side chain of Asp^{224} of the R5P binding loop as observed in the structure of the bsPRS · mATP · SO_4^{2-} · Cd^{2+} complex, while the other takes a different conformation pointing towards the side chain of Asp^{171} of the PPi binding loop. However, in the presence of ATP, the side chain of Arg^{96} assumes the same conformation in both subunits and forms hydrogen bonds with the adenine N1 of ATP and the side chain of Asp^{224} of the R5P binding loop. It is possible that Arg^{96} may be involved not only in the binding of ATP but also in the binding and release of the product PRPP.

The allosteric site

The enzymatic activity of PRS is regulated by both phosphate and ADP, and the activator phosphate and the inhibitor ADP compete for binding at a common allosteric regulatory site [29]. The allosteric site in bsPRS is located at the interface among three subunits of the hexamer [14]. The allosteric site in hPRS1 is composed of conserved residues Gln^{135}, Asp^{143}, Asn^{144} and Ser^{308}–Phe^{313} of one subunit, residues Lys^{100}–Arg^{104} of the flexible loop of the second subunit, and residues Ser^{47}, Arg^{49}, Ala^{80} and Ser^{81} of the third subunit (Figure 2A). In the structures of both hPRS1 · SO_4^{2-} and hPRS1 · ATP · SO_4^{2-} · Cd^{2+} complexes, this site is occupied by a SO_4^{2-} ion, similar to that in the bsPRS · SO_4^{2-} structure. The bound SO_4^{2-} ion occupies the position of the β-phosphate of ADP and has hydrogen-bonding interactions with the side chains of Ser^{47}, Arg^{49}, Arg^{104}, Ser^{308} and Ser^{310}, the main chains of Val^{109} and Ser^{310}, and two water molecules (Figure 3A).

A novel allosteric site

In the structures of both hPRS1 · SO_4^{2-} and hPRS1 · ATP · SO_4^{2-} · Cd^{2+} complexes, one extra SO_4^{2-} ion is identified in each hPRS1 subunit compared with the bsPRS · SO_4^{2-} structure [14]. This SO_4^{2-} binding site is located at the homodimer interface and positioned between the ATP binding site (about 9 Å away from the ribose moiety of ATP) and the previously defined allosteric site (about 13 Å away from the β-phosphate group of ADP and 5 Å away from the adenine moiety of ADP; Figure 2A). This SO_4^{2-} ion has hydrogen-bonding interactions with the side chains of Ser^{132}, Gln^{135}, Asn^{144} and Tyr^{146} of one subunit, and the main chain amides of Lys^{100}, Asp^{101} and Lys^{102} of the flexible loop of the other subunit as well as a water molecule (Figure 3B). All of the residues involved in binding of the SO_4^{2-} ion (Lys^{100}, Asp^{101}, Lys^{102}, Ser^{132}, Gln^{135}, Asp^{144} and Tyr^{146}) are strictly conserved in other eukaryotic PRSs (except plant PRSs of class II which are not dependent on phosphate for activity and lack of an allosteric site for ADP), but can be replaced by other residues in bacterial PRSs (corresponding to Lys^{105}, Ala^{106}, Arg^{107}, Pro^{137}, Gln^{140}, His^{149} and Met^{151} in bsPRS respectively; see Supplementary Figure S1 at http://www.BiochemJ.org/bj/401/bj4010039add.htm). Binding of this SO_4^{2-} is accompanied by substantial conformational change of the flexible loop at the active site. As discussed above, in the bsPRS structure, the flexible loop is partially disordered and adopts different conformations in the absence or presence of ATP and is entirely ordered only when mADP is bound at the allosteric site [14,30]. However, in the hPRS1 structures, the flexible loop is well-defined in the presence and absence of ATP and adopts an open conformation similar to that in the bsPRS · mATP · SO_4^{2-} · Cd^{2+} structure. It was suggested that binding of the metal ion at the active site might induce conformational change and stabilize the open conformation of the flexible loop [30]. However, from analysis of the hPRS1 structures and its comparison with the bsPRS structures, it is apparent that the binding of the extra SO_4^{2-} induces the conformation change at the active site and stabilizes the open conformation of the flexible loop. Since this SO_4^{2-} binding site is very close to the active site and the flexible loop plays an important role in ATP binding and catalysis, we were tempted to speculate that it might be a novel allosteric site for hPRS1.

To investigate this possibility, we performed enzymatic activity assays of both wild-type and mutant hPRS1s containing mutations of some residues at this putative allosteric site (Figure 3C). As described above, the SO_4^{2-} ion at the tentative allosteric site of hPRS1 has hydrogen-bonding interactions with the side chains of Ser^{132}, Gln^{135}, Asn^{144} and Tyr^{146}. All four residues are strictly conserved in eukaryotic PRSs (see Supplementary Figure S1 at http://www.BiochemJ.org/bj/401/bj4010039add.htm). However, Ser^{132} of hPRS1 has a conserved glutamic acid residue in most of the bacterial PRSs but a proline residue (Pro^{137}) in bsPRS; Gln^{135} remains unchanged in all bacterial PRSs; Asn^{144} is conserved in most bacterial PRSs except bsPRS which has a histidine residue (His^{149}) at the equivalent position; and Tyr^{146} has a conserved phenylalanine residue at the equivalent position in most bacterial PRSs but has a methionine residue (Met^{151}) in bsPRS. The mutagenesis results showed that the mutation of Ser^{132} to alanine substantially reduced the enzymatic activity at a low concentration of phosphate (5 mM), but the impairment could be restored to a comparable level with that of wild-type hPRS1 at a high concentration of phosphate (50 mM). However, mutation of Ser^{132} to phenylalanine appeared to have a less significant effect on the enzyme activity at both low and high concentrations of phosphate. Similarly, mutation of Tyr^{146} to methionine (the corresponding residue in bsPRS) caused a marked reduction of the activity at both concentrations of phosphate, but a change of Tyr^{146} to phenylalanine had no substantial effect on the enzyme activity at both concentrations of phosphate. On the other hand, mutation of Asn^{144} to histidine (the corresponding residue in bsPRS) appeared to have no obvious effect on the enzyme activity at both concentrations of phosphate. The enzyme activity of both wild-type and mutant hPRS1s can be inhibited by ADP.

At the same time, we determined the crystal structures of S132A and Y146M mutant hPRS1s. The overall structures of the two mutants are almost identical with that of wild-type hPRS1 except for very fine conformational differences at the SO_4^{2-} binding site (Figure 3D). In the S132A mutant structure, the SO_4^{2-} lost a hydrogen bond with the side chain of Ser^{132}, but retained a hydrogen bond with the main chain carbonyl of Ala^{132} via a water molecule compared with the wild-type hPRS1 structure. This may explain the biochemical data that the binding of phosphate (or SO_4^{2-}) with the S132A mutant is weakened at low concentrations of the activator due to the loss of the side chain interaction, but can be restored at high concentrations of the activator because of the preservation of the main chain interaction. In the Y146M mutant structure, the new SO_4^{2-} binding site is fully occupied by a SO_4^{2-} ion in one subunit, but partially occupied with a low occupancy (0.5) in the other. Moreover, in the latter subunit, the surrounding residues interacting with the SO_4^{2-} ion have relatively higher B factors, an indication of higher flexibility. These results indicate that the binding of the SO_4^{2-} ion is weaker in at least one subunit of the homodimer due to Y146M mutation, consistent with the biochemical data that mutation Y146M resulted in a decrease in the enzyme activity. A modelling study also shows that mutation

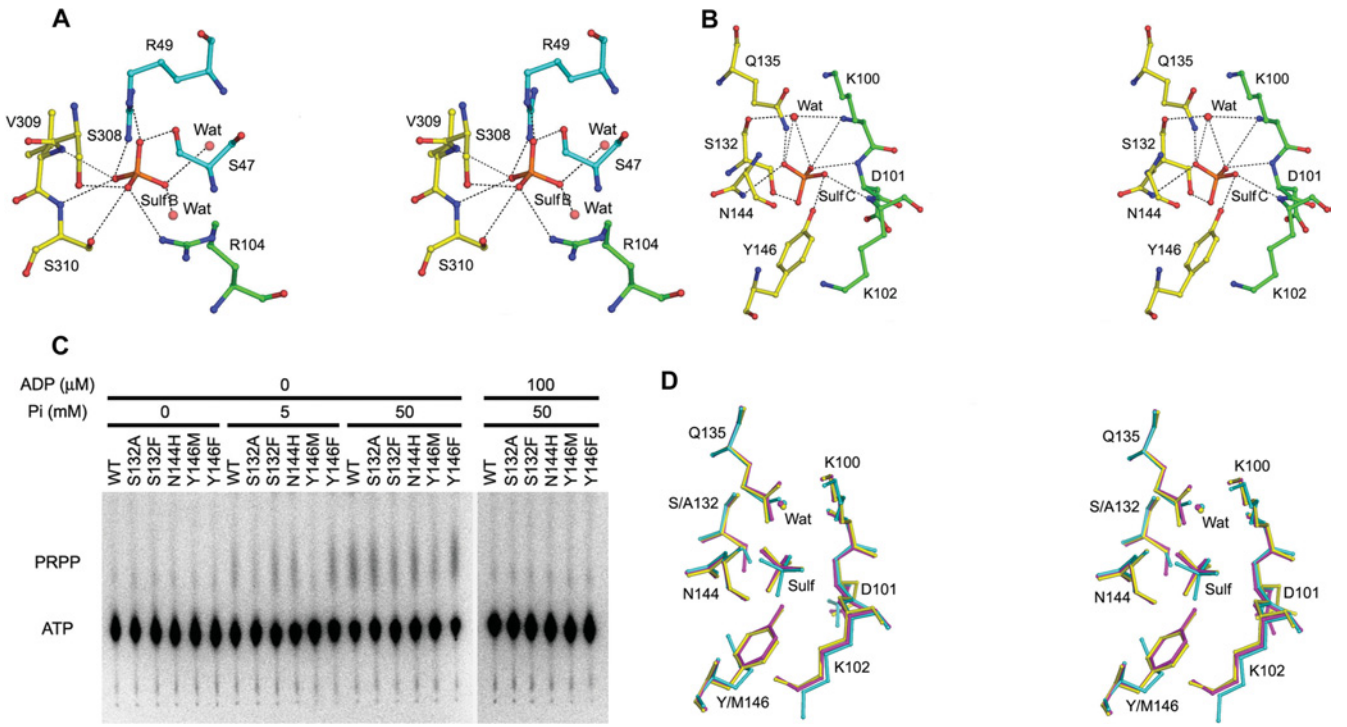

Figure 3 Structures of the allosteric sites

(**A**) Interactions of the SO_4^{2-} ion with the surrounding residues at the previously defined allosteric site (Sulf B). Residues of the three subunits forming the allosteric site are shown in yellow, green and cyan respectively. The hydrogen-bonding interactions are indicated with thin dashed lines. (**B**) Interactions of the SO_4^{2-} ion with the surrounding residues at the new allosteric site (Sulf C). Residues of the two different subunits forming this allosteric site are shown in yellow and green respectively. (**C**) Activity assay of wild-type and mutant hPRS1s. All the lanes are incubated and developed at the same conditions. All experiments were performed at least three times with comparable results. (**D**) Structural comparison of wild-type and the S132A and Y146M mutant hPRS1s at the new allosteric site (Sulf C). The wild-type hPRS1 is shown in magenta, the S132A mutant in yellow, and the Y146M mutant in cyan.

of Asn^{144} to histidine could maintain a hydrogen bond between the side chain and the SO_4^{2-} ion and therefore, has no significant effect on the activity. Taking the structural and biochemical data together, we suggest that this new SO_4^{2-} binding site is a second allosteric site which can regulate the enzymatic activity.

Implications for the allosteric regulatory mechanism

The crystal structures of hPRS1 complexes with SO_4^{2-} and with ATP, together with the biochemical data, have revealed a second allosteric site in addition to the allosteric site defined previously in bsPRS. Binding of the activator SO_4^{2-} to the new allosteric site stabilizes the flexible loop, an important structural element involved in Mg–ATP binding, resulting in the formation of the active, open conformation similar to that in the structure of the bsPRS · mADP complex [30]. This stabilization is essential to the binding of the substrate Mg–ATP and the initiation of the catalytic reaction. Moreover, binding of the activator SO_4^{2-} to the second allosteric site brings the flexible loop closer to its co-ordination sphere which makes the tip of the loop in partial overlap with the binding site of the adenine moiety of ADP and prevents entering and/or binding of the inhibitor ADP, leading to the activation of the enzyme. Conversely, binding of the inhibitor ADP to the first allosteric site would block the second allosteric site and prevent conformational rearrangement of structural elements at the active site, leading to the inhibition of the enzyme. This is the first time that structural stabilization at the active site induced by binding of the activator SO_4^{2-} to the allosteric sites has been observed. Since the residues forming the second allosteric site are strictly conserved in eukaryotic PRSs (except class II plant PRSs), but can be replaced by other residues in bacterial PRSs, it seems plausible that this new allosteric site might also exist in other eukaryotic PRSs, but not in bacterial PRSs. This second allosteric site might be developed during evolution to provide a very fine regulatory mechanism of the enzymatic activity for eukaryotic PRSs because of the complexity of cellular activity in eukaryotes.

We thank the staff members at Photon Factory, Japan, for technical support in diffraction data collection; Qiuhua Huang of Shanghai Institute of Hematology, Rui-jin Hospital, for providing human PRS1 plasmid; Dr Jinqiu Zhou for assistance in enzymatic activity assay; and other members of our group for helpful discussion. This work was supported by NSFC grants (30125011 and 30570379), MOST 973 and 863 grants (2002BA711A13, 2004CB520801, and 2004CB720102), and CAS grant (KSCX1-SW-17).

REFERENCES

1 Kornberg, A., Lieberman, I. and Simms, E. S. (1955) Enzymatic synthesis and properties of 5-phosphoribosylpyrophosphate. J. Biol. Chem. **215**, 389–402
2 Khorana, H. G., Fernandes, J. F. and Kornberg, A. (1958) Pyrophosphorylation of ribose 5-phosphate in the enzymatic synthesis of 5-phosphorylribose 1-pyrophosphate. J. Biol. Chem. **230**, 941–948
3 Miller, Jr, G. A., Rosenzweig, S. and Switzer, R. L. (1975) Oxygen-18 studies of the mechanism of pyrophosphoryl group transfer catalyzed by phosphoribosylpyrophosphate synthetase. Arch. Biochem. Biophys. **171**, 732–736
4 Hove-Jensen, B. (1988) Mutation in the phosphoribosylpyrophosphate synthetase gene (prs) that results in simultaneous requirements for purine and pyrimidine nucleosides, nicotinamide nucleotide, histidine and tryptophan in *Escherichia coli*. J. Bacteriol. **170**, 1148–1152
5 Hove-Jensen, B. (1989) Phosphoribosylpyrophosphate (PRPP)-less mutants of *Escherichia coli*. Mol. Microbiol. **3**, 1487–1492

6 Yen, R. C., Adams, W. B., Lazar, C. and Becker, M. A. (1978) Evidence for X-linkage of human phosphoribosylpyrophosphate synthetase. Proc. Natl. Acad. Sci. U.S.A. **75**, 482–485

7 Zoref, E., De Vries, A. and Sperling, O. (1975) Mutant feedback-resistant phosphoribosylpyrophosphate synthetase associated with purine overproduction and gout. Phosphoribosylpyrophosphate and purine metabolism in cultured fibroblasts. J. Clin. Invest. **56**, 1093–1099

8 Becker, M. A., Losman, M. J. and Kim, M. (1987) Mechanisms of accelerated purine nucleotide synthesis in human fibroblasts with superactive phosphoribosylpyrophosphate synthetases. J. Biol. Chem. **262**, 5596–5602

9 Roessler, B. J., Nosal, J. M., Smith, P. R., Heidler, S. A., Palella, T. D., Switzer, R. L. and Becker, M. A. (1993) Human X-linked phosphoribosylpyrophosphate synthetase superactivity is associated with distinct point mutations in the PRPS1 gene. J. Biol. Chem. **268**, 26476–26481

10 Becker, M. A., Smith, P. R., Taylor, W., Mustafi, R. and Switzer, R. L. (1995) The genetic and functional basis of purine nucleotide feedback-resistant phosphoribosyl-pyrophosphate synthetase superactivity. J. Clin. Invest. **96**, 2133–2141

11 Krath, B. N., Eriksen, T. A., Poulsen, T. S. and Hove-Jensen, B. (1999) Cloning and sequencing of cDNAs specifying a novel class of phosphoribosyl diphosphate synthase in *Arabidopsis thaliana*. Biochim. Biophys. Acta **1430**, 403–408

12 Krath, B. N. and Hove-Jensen, B. (2001) Class II recombinant phosphoribosyl diphosphate synthase from spinach. Phosphate independence and diphosphoryl donor specificity. J. Biol. Chem. **276**, 17851–17856

13 Krath, B. N. and Hove-Jensen, B. (2001) Implications of secondary structure prediction and amino acid sequence comparison of class I and class II phosphoribosyl diphosphate synthases on catalysis, regulation, and quaternary structure. Protein Sci. **10**, 2317–2324

14 Eriksen, T. A., Kadziola, A., Bentsen, A. K., Harlow, K. W. and Larsen, S. (2000) Structural basis for the function of *Bacillus subtilis* phosphoribosyl-pyrophosphate synthetase. Nat. Struct. Biol. **7**, 303–308

15 Kadziola, A., Jepsen, C. H., Johansson, E., McGuire, J., Larsen, S. and Hove-Jensen, B. (2005) Novel class III phosphoribosyl diphosphate synthase structure and properties of the tetrameric, phosphate-activated, non-allosterically inhibited enzyme from *Methanocaldococcus jannaschii*. J. Mol. Biol. **354**, 815–828

16 Switzer, R. L. (1969) Regulation and mechanism of phosphoribosylpyrophosphate synthetase. I. Purification and properties of the enzyme from *Salmonella typhimurium*. J. Biol. Chem. **244**, 2854–2863

17 Fox, I. H. and Kelley, W. N. (1971) Human phosphoribosylpyrophosphate synthetase. Distribution, purification, and properties. J. Biol. Chem. **246**, 5739–5748

18 Switzer, R. L. and Sogin, D. C. (1973) Regulation and mechanism of phosphoribosylpyrophosphate synthetase. V. Inhibition by end products and regulation by adenosine diphosphate. J. Biol. Chem. **248**, 1063–1073

19 Roth, D. G., Shelton, E. and Deuel, T. F. (1974) Purification and properties of phosphoribosyl pyrophosphate synthetase from rat liver. J. Biol. Chem. **249**, 291–296

20 Roth, D. G. and Deuel, T. F. (1974) Stability and regulation of phosphoribosyl pyrophosphate synthetase from rat liver. J. Biol. Chem. **249**, 297–301

21 Gibson, K. J., Schubert, K. R. and Switzer, R. L. (1982) Binding of the substrates and the allosteric inhibitor adenosine 5′-diphosphate to phosphoribosylpyrophosphate synthetase from *Salmonella typhimurium*. J. Biol. Chem. **257**, 2391–2396

22 Hove-Jensen, B., Harlow, K. W., King, C. J. and Switzer, R. L. (1986) Phosphoribosylpyrophosphate synthetase of Escherichia coli. Properties of the purified enzyme and primary structure of the prs gene. J. Biol. Chem. **261**, 6765–6771

23 Kita, K., Otsuki, T., Ishizuka, T., Ishijima, S. and Tatibana, M. (1989) Rat liver phosphoribosylpyrophosphate synthetase: existence as heterogeneous aggregates and identification of the catalytic subunit. Adv. Exp. Med. Biol. **253**, 1–6

24 Arnvig, K., Hove-Jensen, B. and Switzer, R. L. (1990) Purification and properties of phosphoribosyl-diphosphate synthetase from *Bacillus subtilis*. Eur. J. Biochem. **192**, 195–200

25 Fox, I. H. and Kelley, W. N. (1972) Human phosphoribosylpyrophosphate synthetase. Kinetic mechanism and end product inhibition. J. Biol. Chem. **247**, 2126–2131

26 Willemoes, M. and Hove-Jensen, B. (1997) Binding of divalent magnesium by *Escherichia coli* phosphoribosyl diphosphate synthetase. Biochemistry **36**, 5078–5083

27 Meyer, L. J. and Becker, M. A. (1977) Human erythrocyte phosphoribosylpyrophosphate synthetase. Dependence of activity on state of subunit association. J. Biol. Chem. **252**, 3919–3925

28 Becker, M. A., Kostel, P. J. and Meyer, L. J. (1975) Human phosphoribosylpyrophosphate synthetase. Comparison of purified normal and mutant enzymes. J. Biol. Chem. **250**, 6822–6830

29 Willemoes, M., Hove-Jensen, B. and Larsen, S. (2000) Steady state kinetic model for the binding of substrates and allosteric effectors to *Escherichia coli* phosphoribosyl-diphosphate synthase. J. Biol. Chem. **275**, 35408–35412

30 Eriksen, T. A., Kadziola, A. and Larsen, S. (2002) Binding of cations in *Bacillus subtilis* phosphoribosyldiphosphate synthetase and their role in catalysis. Protein Sci. **11**, 271–279

31 Iizasa, T., Taira, M., Shimada, H., Ishijima, S. and Tatibana, M. (1989) Molecular cloning and sequencing of human cDNA for phosphoribosylpyrophosphate synthetase subunit II. FEBS Lett. **244**, 47–50

32 Sonoda, T., Taira, M., Ishijima, S., Ishizuka, T., Iizasa, T. and Tatibana, M. (1991) Complete nucleotide sequence of human phosphoribosylpyrophosphate synthetase subunit I (PRSI) cDNA and a comparison with human and rat PRPS gene families. J. Biochem. **109**, 361–364

33 Taira, M., Iizasa, T., Shimada, H., Kudoh, J., Shimizu, N. and Tatibana, M. (1990) A human testis-specific mRNA for phosphoribosylpyrophosphate synthetase that initiates from a non-AUG codon. J. Biol. Chem. **265**, 16491–16497

34 Nosal, J. M., Switzer, R. L. and Becker, M. A. (1993) Overexpression, purification, and characterization of recombinant human 5-phosphoribosyl-pyrophosphate synthetase isozymes I and II. J. Biol. Chem. **268**, 10168–10175

35 Fox, I. H. and Kelley, W. N. (1973) Human phosphoribosylpyrophosphate (PP-ribose-P) synthetase: properties and regulation. Adv. Exp. Med. Biol. **41**, 79–86

36 Tang, W., Li, X., Zhu, Z., Tong, S., Li, X., Zhang, X., Teng, M. and Niu, L. (2006) Expression, purification, crystallization and preliminary X-ray diffraction analysis of human phosphoribosyl pyrophosphate synthetase 1 (PRS1). Acta Cryst. **F62**, 432–434

37 Zhang, Q. H., Ye, M., Wu, X. Y., Ren, S. X., Zhao, M., Zhao, C. J., Fu, G., Shen, Y., Fan, H. Y., Lu, G. et al. (2000) Cloning and functional analysis of cDNAs with open reading frames for 300 previously undefined genes expressed in CD34+ hematopoietic stem/progenitor cells. Genome Res. **10**, 1546–1560

38 Brunger, A. T., Adams, P. D., Clore, G. M., DeLano, W. L., Gros, P., Grosse-Kunstleve, R. W., Jiang, J. S., Kuszewski, J., Nilges, M., Pannu, N. S. et al. (1998) Crystallography and NMR system: a new software suite for macromolecular structure determination. Acta Cryst. **D54**, 905–921

39 Murshudov, G. N., Vagin, A. A. and Dodson, E. J. (1997) Refinement of macromolecular structures by the maximum-likelihood method. Acta Cryst. **D53**, 240–255

40 Jones, T. A., Zou, J. Y., Cowan, S. W. and Kjeldgaard, M. (1991) Improved methods for building protein models in electron density maps and the location of errors in these models. Acta Cryst. **A47**, 110–119

41 Jensen, K. F., Houlberg, U. and Nygaard, P. (1979) Thin-layer chromatographic methods to isolate 32P-labeled 5-phosphoribosyl-α-1-pyrophosphate (PRPP): determination of cellular PRPP pools and assay of PRPP synthetase activity. Anal. Biochem. **98**, 254–263

42 Schubert, K. R., Switzer, R. L. and Shelton, E. (1975) Studies of the quaternary structure and the chemical properties of phosphoribosylpyrophosphate synthetase from Salmonella typhimurium. J. Biol. Chem. **250**, 7492–7500

43 Hove-Jensen, B., Bentsen, A.-K. K. and Harlow, K. W. (2005) Catalytic residues Lys197 and Arg199 of *Bacillus subtilis* phosphoribosyl diphosphate synthetase: alanine-scanning mutagenesis of the flexible catalytic loop. FEBS J. **272**, 3631–3639

44 Liao, J. C., Sun, S., Chandler, D. and Oster, G. (2004) The conformational states of Mg. ATP in water. Eur. Biophys. J. **33**, 29–37

45 Focia, P. J., Craig, 3rd, S. P., Nieves-Alicea, R., Fletterick, R. J. and Eakin, A. E. (1998) A 1.4 Å crystal structure for the hypoxanthine phosphoribosyltransferase of *Trypanosoma cruzi*. Biochemistry **37**, 15066–15075

46 Shi, W., Munagala, N. R., Wang, C. C., Li, C. M., Tyler, P. C., Furneaux, R. H., Grubmeyer, C., Schramm, V. L. and Almo, S. C. (2000) Crystal structures of *Giardia lamblia* guanine phosphoribosyltransferase at 1.75 Å. Biochemistry **39**, 6781–6790

Received 13 July 2006/16 August 2006; accepted 30 August 2006
Published as BJ Immediate Publication 30 August 2006, doi:10.1042/BJ20061066